Joint Satellite Code and Carrier Tracking

Kaspar Giger, Patrick Henkel, *Technische Universität München*
Christoph Günther, *German Aerospace Center (DLR)*

BIOGRAPHIES

Kaspar Giger received the M.S. degree in electrical engineering and information technology from the Swiss Federal Institute of Technology (ETH), Zurich, Switzerland, in 2006. In his M.S. thesis, he worked on an implementation and optimization of a real-time MPEG4/AVC H.264 encoder on a TI DM642 DSP platform. He is currently pursuing the Ph.D. degree at the Institute for Communications and Navigation, Technische Universität München, Munich, Germany, working on new signal tracking algorithms.

Patrick Henkel studied electrical engineering and information technology at the Technische Universität München, Munich, Germany, and the Ecole Polytechnique de Montreal, Montreal, Canada. He is currently pursuing the Ph.D. degree at the Institute for Communications and Navigation, TUM, and his focus is on robust ambiguity resolution for precise carrier-phase positioning with multiple frequencies. In 2007, he was a Guest Researcher at TU Delft, Netherlands, in 2008 at the GPS Lab at Stanford University, USA. Mr. Henkel received the Pierre Contensou Gold Medal at the International Astronautical Congress in 2007.

Christoph Günther studied theoretical physics at the Swiss Federal Institute of Technology (ETH), Zurich, Switzerland. He received his diploma in 1979 and completed his PhD in 1984. He worked on communication and information theory at Brown Boveri and Ascom Tech. From 1995, he led the development of mobile phones for GSM and later dual mode GSM/Satellite phones at Ascom. In 1999, he became head of the research department of Ericsson in Nuremberg. Since 2003, he is the director of the Institute of Communications and Navigation at the German Aerospace Center (DLR) and since December 2004, he additionally holds a Chair at the Technische Universität München, Munich, Germany. His research interests are in satellite navigation, communication, and signal processing.

ABSTRACT

Current GNSS receivers employ independent tracking loop for each received signal, i.e. every satellite and every frequency. With this receiver design a time consuming re-acquisition is needed, whenever a signal is temporarily lost. By formulating the tracking process jointly for all signals, given the involved random processes, such as receiver movements, receiver clock and atmospherical effects, the spatial and spectral correlation of the signals can be exploited. The joint tracking method was tested in an airborne receiver during two stages of flight. In the comparison to a commercial receiver the joint tracking receiver shows its great potential by continuously tracking all signals. This led us to the conclusion that a joint satellite code and carrier tracking receiver makes a GNSS receiver more robust, especially airborne receivers.

1. INTRODUCTION

Today a GNSS receiver receives signals from multiple satellites and on multiple frequencies, where the satellites belong to different navigation systems, e.g. GPS, Galileo (starting with the GIOVE satellites), ... The receiver typically sets up phase and delay locked loops (PLL, DLL) for every signal [1]. To further increase the precision of the code-tracking, the carrier-aided DLL is often implemented. In a dual-frequency receiver the carrier on one frequency is in addition also used to aid the tracking on the second frequency (e.g. L2).

Whenever a satellite is masked or suffers from a strong attenuation (e.g. excited by ionospheric scintillation) the receiver loses lock of the carrier-phase synchronization, e.g. [2]. After a loss of lock the receiver falls back into frequency tracking mode or even discards the tracking of the satellite. A following re-acquisition and re-synchronization is first of all time consuming and secondly leads to a changed integer ambiguity of the carrier-phase. But GNSS receivers using carrier-phase positioning only get a high precision by relying on a constant ambiguity [3].

To increase the robustness of the GNSS receiver, especially in the described environments, the spatial correlation of the signals was exploited by Sennott and Senffner in [4]. Spilker developed a similar idea for the code tracking loop in the Vector DLL [5]. The idea of vector tracking recently gained interest together with the first software defined GNSS receivers, e.g. [6]. Henkel et al. proposed

to further exploit the spectral correlation of the signals [7].

Until now only the code and frequency was tracked in the VDLL. Aiming at carrier-phase positioning in aircrafts, the methods clearly have to be extended to the phase tracking process and need to be combined with the code tracking. Clearly with the upcoming navigation systems like Galileo, the spectral correlation should also be exploited in the code and carrier tracking. And finally the algorithm should allow the joint tracking of multiple constellations.

The objective of this paper is to introduce the joint tracking loop as a tool to make the carrier- and code-phase tracking in GNSS receivers more robust. In particular we are interested in its use in airborne GNSS receivers. This paper is divided into five sections. After this short introduction follows a detailed formulation of the carrier and code tracking problem in a GNSS receiver. The controller emerging from this model is then employed as the joint satellite code and carrier tracking method. Its performance is evaluated in section 3, followed by a discussion of the results in section 4. The paper is finally concluded in section 5.

2. JOINT CODE AND CARRIER TRACKING

With the advent of software-defined GNSS receivers, the usage of Kalman filters for the tracking in GNSS receivers has recently gained high attention, cf. [8]. In this approach, the received phase is modeled as consisting of a line-of-sight and an oscillator part. Depending on this model, the phase estimation filter can be set up.

Although in this way the optimal phase-estimator can be found, there's no direct hint on how to steer the local oscillator – although this relationship could be derived according to the well-known PLL by using Patapoutian's loop representation [9]. But to have better control of the phase and frequency of the local oscillator, the tracking loop needs to be represented as a control problem [10]. This procedure can be further extended to include the signals from multiple satellites of different constellations, received at multiple frequencies.

In this section the model used to derive the joint phase tracking is detailed. It is followed by the extension to code and carrier tracking, a discussion about observability and controllability and the design of the linear controller.

PHASE MODEL

The true phase of the received signal is first broken down into the parts originating from the receiver motion, the receiver oscillator, the atmosphere and the satellite's oscillator [1]:

$$\varphi_m^k(t) = \omega_c t + \frac{2\pi}{\lambda_m}\Big(\left(\mathbf{e}^k\right)^T \left[\mathbf{r}(t) - \mathbf{r}^k(t')\right] + c\delta(t) + c\delta^k(t') - I_m^k(t'') + T^k(t''')\Big).$$

The following denotations are used:

m	the carrier frequency ($1 \dots M$),
k	the satellite ($1 \dots K$),
$\mathbf{e}^k$	unit vector pointing from the k-th satellite to the receiver,
$\mathbf{r}, \mathbf{r}^k$	the locations of the receiver and satellite k in the same Cartesian coordinate system (e.g. ECEF),
δ, δ^k	the receiver and satellite clock bias (in seconds),
I_m^k	the ionospheric delay (in meters),
T^k	the tropospheric delay (in meters),
t'	the time when the signal (received at time t) was emitted,
t''	the time when the signal hit the ionosphere (simplifying the ionosphere as a thin shell) and
t'''	the time when the signal hit the troposphere (same simplification).

Each of the parts is modeled as a random walk, driven by white Gaussian noise [11]. Denoting by n_x the order of the derivative represented by the noise sequence ($x^{(n_x)}(t) = w_x(t)$), Taylor's theorem can be used to characterize the evolution over time of the process $x(t)$:

$$x(t+T) = \sum_{l=0}^{n_x-1} x^{(l)}(t)\frac{T^l}{l!} + R_x(t, t+T, n_x), \qquad (1)$$

defining the general remainder term as

$$R_x(t_1, t_2, l) = \int_{t_1}^{t_2} w_x(u)\frac{(t_2-u)^{n_x-l-1}}{(n_x-l-1)!}du.$$

The same expansion can clearly be carried out for higher derivatives of $x(t)$. All the derivatives stacked into a vector, result in

$$\underbrace{\begin{bmatrix} x^{(0)}(t_{i+1}) \\ \vdots \\ x^{(n_x-1)}(t_{i+1}) \end{bmatrix}}_{\mathbf{x}_x(t_{i+1})} = \mathbf{A}_{n_x}\mathbf{x}_x(t_i) + \underbrace{\begin{bmatrix} R_x(t_i, t_{i+1}, n_x) \\ \vdots \\ R_x(t_i, t_{i+1}, 1) \end{bmatrix}}_{\mathbf{w}_{x,i+1}},$$

$$\text{with } (\mathbf{A}_{n_x})_{h,j} = \begin{cases} \frac{T^{j-h}}{(j-h)!}, & \text{if } j-h \geq 0 \\ 0 & \text{otherwise} \end{cases}$$

$$\text{and } T = t_{i+1} - t_i.$$

Plugging in the expansions for the above mentioned processes influencing the signal phase, a state-space model

for the received signal phase emerges

$$\begin{aligned}\boldsymbol{\varphi}^k_{m,i+1} &= \mathbf{x}_{\phi,i+1} + \left(\mathbf{e}^k\right)^T \otimes \mathbf{I}_{n_r}\left(\mathbf{x}_{r,i+1} - \mathbf{x}_{r^k,i+1}\right) \\ &\quad + \mathbf{x}_{\delta,i+1} + \mathbf{x}_{\delta^k,i+1} - \mathbf{x}_{I^k_m,i+1} + \mathbf{x}_{T^k,i+1} \\ &= \mathbf{A}_n\Big(\mathbf{x}_{\phi,i} + \left(\mathbf{e}^k\right)^T \otimes \mathbf{I}_n\left(\mathbf{x}_{r,i} - \mathbf{x}_{r^k,i}\right) \\ &\quad + \mathbf{x}_{\delta,i} + \mathbf{x}_{\delta^k,i} - \mathbf{x}_{I^k_m,i} + \mathbf{x}_{T^k,i}\Big) \\ &\quad + \frac{2\pi}{\lambda_m}\Big(\left(\mathbf{e}^k\right)^T \otimes \mathbf{I}_n\left(\mathbf{w}_{r,i+1} - \mathbf{w}_{r^k,i+1}\right) \\ &\quad + \mathbf{w}_{\delta,i+1} + \mathbf{w}_{\delta^k,i+1} - \mathbf{w}_{I^k_m,i+1} + \mathbf{w}_{T^k,i+1}\Big)\end{aligned} \tag{2}$$

having $n = \max\left(n_\phi, n_r, n_{r^k}, n_\delta, n_{\delta^k}, n_I, n_T\right)$.

Not all of the processes have the order n. The state-vector of those with reduced order are augmented by a sufficient number of zero-valued entries.

NCO MODEL

In analogy to the beforehand derived model for the received signal phase (and its derivatives), a model for the Numerically Controlled Oscillator has to be found. In contrast to the phase-model, the states of the NCO are driven by a user-defined input signal rather than (process) noise.

Allowing the frequency and the phase to be changed between successive integration intervals, the following NCO model arises:

$$\underbrace{\begin{bmatrix} \varphi^k_{\text{NCO},m,i+1} \\ \omega^k_{\text{NCO},m,i+1} \\ 0 \\ \vdots \end{bmatrix}}_{\boldsymbol{\varphi}^k_{\text{NCO},m,i+1}} = \mathbf{A}_n \boldsymbol{\varphi}^k_{\text{NCO},m,i} + \underbrace{\begin{bmatrix} \mathbf{I}_2 \\ \mathbf{0} \end{bmatrix}}_{-\mathbf{B}_0} \mathbf{u}^k_{\varphi,m,i} \tag{3}$$

The state-vector of the NCO could as well be augmented by higher order derivatives of the NCO-phase, leading to a higher order NCO. However in this text only second-order NCOs are considered.

PLANT MODEL

As proposed by [12], a plant model for the individual phase control system can be found by taking the difference of Equations 2 and 3:

$$\begin{aligned}\underbrace{\left(\boldsymbol{\varphi}^k_{m,i+1} - \boldsymbol{\varphi}^k_{\text{NCO},m,i+1}\right)}_{\mathbf{x}^k_{\varphi,m,i+1}} = \;& \mathbf{A}_n \mathbf{x}^k_{\varphi,m,i} + \tfrac{2\pi}{\lambda_m}\Big(\left(\mathbf{e}^k\right)^T \otimes \mathbf{I}_{n_r} \\ & \cdot \left(\mathbf{w}_{r,i+1} - \mathbf{w}_{r^k,i+1}\right) \\ & + \mathbf{w}_{\delta,i+1} + \mathbf{w}_{\delta^k,i+1} \\ & - \mathbf{w}_{I^k_m,i+1} + \mathbf{w}_{T^k,i+1}\Big) \\ & + \mathbf{B}_0 \mathbf{u}^k_{\varphi,m,i}\end{aligned} \tag{6}$$

Taking a closer look at the noise terms (or remainder terms of the Taylor expansion) in the above model, we see that the contributions from several satellites/frequencies are correlated or simply scaled.

Receiver movements Assuming uncorrelated movements in the three spatial dimensions, their projection onto the line-of-sight vector is observed in the phase-domain:

$$\varphi^k_{r_m}(t) = \frac{2\pi}{\lambda_m}\left(\left(\mathbf{e}^k\right)^T \mathbf{r}(t)\right)$$

The Taylor expansion like performed in Equation 1 is in theory not valid, since the unit vector $\mathbf{e}^k$ might be changing during the interval of consideration. The expected rate of change is in the order of less than 10^{-3} per second and can therefore be neglected in this analysis. Hence, the noise terms are just scaled by the unit vectors at the beginning of the interval.

Satellite movements The movements of the satellites are given with a high and sufficient precision (e.g. Broadcast or IGS ephemerides). Due to their smooth dynamics the satellites can be modeled as having a constant acceleration over the interval of consideration. The remainder terms of the Taylor series are then simplified as

$$\begin{aligned}R_{r^k_x}(t_i, t_{i+1}, l) &= \int_{t_i}^{t_{i+1}} \dddot{\mathbf{r}}^k_x(u)\frac{(t_{i+1}-u)^{l-1}}{(l-1)!}du \\ &\approx \dddot{\mathbf{r}}^k_x(t_i)\frac{T^l}{(l-1)!\cdot l}, \qquad l \in \{2,1\}\end{aligned}$$

The impact of the satellite movements is therefore deterministic and can be seen as a reference input to the phase-system. As we want to follow the phase of the received signal, the same input has to be used for the local system, i.e. the NCO:

$$\mathbf{u}^k_{\text{ref.},m,i} = \frac{2\pi}{\lambda_m}\left(\mathbf{e}^k\right)^T \ddot{\mathbf{r}}^k_i \begin{bmatrix} T^2/2 \\ T \end{bmatrix}.$$

Ionospheric delay For any satellite, the ionospheric delay is scaled with the carrier frequency – neglecting higher order ionospheric effects. Therefore the remainder terms in Equation 6 are scaled by their frequency-factor q:

$$\text{with } I^k_m(t) = q_m^2 I^k_0(t), \text{ and } q_m = \frac{f_0}{f_m}:$$

$$\left(\mathbf{w}_{I^k_m,i+1}\right)_l = \begin{cases} q_m^2 R_{I^k_0}(t_i, t_{i+1}, n_I - l + 1), \\ \qquad\qquad \text{for } l = 1, \ldots, n_I \\ 0, \qquad\qquad \text{otherwise} \end{cases}$$

$$\mathbf{G}_\varphi = 2\pi \cdot \left[\begin{array}{c:c:ccc:ccc:ccc} \boldsymbol{\mu}\otimes\left(\mathbf{e}^1\right)^T & \boldsymbol{\mu} & \boldsymbol{\mu} & \mathbf{0} & \dots & -\mathbf{q}\cdot\boldsymbol{\mu} & \mathbf{0} & \dots & m^1\boldsymbol{\mu} & \mathbf{0} & \dots \\ \boldsymbol{\mu}\otimes\left(\mathbf{e}^2\right)^T & \boldsymbol{\mu} & \mathbf{0} & \boldsymbol{\mu} & & \mathbf{0} & -\mathbf{q}\cdot\boldsymbol{\mu} & & \mathbf{0} & m^2\boldsymbol{\mu} & \\ \vdots & \vdots & \vdots & & \ddots & \vdots & & \ddots & \vdots & & \ddots \end{array}\right] \otimes \mathbf{I}_n \tag{4}$$

$$= 2\pi \cdot \left[\mathbf{H}\otimes\boldsymbol{\mu},\ \mathbf{I}_K\otimes\boldsymbol{\mu},\ -\mathbf{I}_K\otimes(\mathbf{q}\cdot\boldsymbol{\mu}),\ \operatorname{diag}\left(m^1,\dots,m^K\right)\otimes\boldsymbol{\mu}\right]\otimes\mathbf{I}_n \tag{5}$$

Tropospheric delay The tropospheric delay encountered by the signals received from a satellite can be mapped to the receiver's tropospheric zenith delay [1]:

$$T^k(t) = m^k(t)\cdot T_Z(t)$$

Like in the preceding paragraphs the Taylor expansion is also performed for the tropospheric zenith delay, with the simplifying assumption that the mapping function is constant during the considered interval.

The plant model can now be summarized to be

$$\mathbf{x}_{\varphi,i+1} = \mathbf{A}\mathbf{x}_{\varphi,i} + \mathbf{B}\mathbf{u}_{\varphi,i} + \mathbf{G}_\varphi\mathbf{w}_{i+1},$$

with

$$\begin{aligned}
\mathbf{A} &= \mathbf{I}_{K\cdot M}\otimes\mathbf{A}_n,\\
\mathbf{B} &= \mathbf{I}_{K\cdot M}\otimes\mathbf{B}_0,\\
\mathbf{w}_i &= \left[\mathbf{w}_{r,i}^T,\ \mathbf{w}_{\delta,i}^T,\ \mathbf{w}_{\delta^1,i}^T,\ \mathbf{w}_{\delta^2,i}^T,\ \dots,\right.\\
&\qquad \left.\mathbf{w}_{I_0^1,i},\ \mathbf{w}_{I_0^2,i},\ \dots,\ \mathbf{w}_{T_Z,i}\right]^T,\\
\boldsymbol{\mu} &= \left[\frac{1}{\lambda_1},\dots,\frac{1}{\lambda_M}\right]^T,\\
\mathbf{q} &= \operatorname{diag}\left[q_1^2,\dots,q_M^2\right]^T,
\end{aligned}$$

and the matrix $\mathbf{G}_\varphi$ as defined in Equation 4. Additionally the covariance of the process noise vector $\mathbf{w}_{i+1}$ has to be defined. By following the approach described above, the covariance matrix can be found in a way, similar to [13].

As the states are not directly observable, they need to be estimated by an observer (typically implemented as a Kalman filter). The outcome of the phase-discriminator can be used as the measurement for the observer:

$$D_{\varphi,m,i}^k = \operatorname{atan}\left(\frac{Q_{m,i}^k}{I_{m,i}^k}\right) \approx \overline{\Delta\varphi_{m,i}^k} + n_{\varphi,m,i}^k, \tag{7}$$

where $\overline{\Delta\varphi_{m,i}^k}$ denotes the average phase error during the interval $[t_{i-1}, t_i]$ and $n_{\varphi,m,i}^k$ is the measurement noise. As derived in the appendix, the covariance of these measurements is given as

$$\mathbb{E}\left\{n_{\varphi,m,i}^k n_{\varphi,m,j}^k\right\} = \delta(i-j)\cdot\frac{1}{2C_m^k/N_0T}.$$

In the case of multisatellite and multifrequency tracking a set of measurements is used to estimate the states:

$$\begin{aligned}
&\left[D_{\varphi,m=1,i}^{k=1},\ D_{\varphi,2,i}^1,\ \dots,\ D_{\varphi,1,i}^2,\ \dots\right]^T\\
&\qquad = \underbrace{\left(\mathbf{I}_{M\cdot K}\otimes\mathbf{C}_n\right)}_{\mathbf{C}}\mathbf{x}_{\varphi,i} + \mathbf{n}_{\varphi,i},
\end{aligned} \tag{8}$$

with the well known observation matrix $\mathbf{C}_n$, with $\left(\mathbf{C}_n\right)_{1,j} = T^{j-1}/j!,\ j = 1,\dots,n$ (e.g. [8]).

JOINT CODE- AND CARRIER-PHASE MODEL

In a similar way like the derivation of a carrier-phase model in the previous section, a model for the code-phase can be derived as well. This ensures continuous signal-tracking in the receiver. As derived in [14], the basic difference is the reversed sign of the ionospheric delay and a different scaling of the remainder terms:

$$\begin{aligned}
\mathbf{x}_{\tau,m,i+1}^k = \mathbf{A}_n\mathbf{x}_{\tau,m,i}^k + \frac{f_{\text{code},m}}{c}\Big(&\left(\mathbf{e}^k\right)^T\otimes\mathbf{I}_{n_r}\\
&\cdot\left(\mathbf{w}_{r,i+1} - \mathbf{w}_{r^k,i+1}\right) + \mathbf{w}_{\delta,i+1} + \mathbf{w}_{\delta^k,i+1}\\
&+ \mathbf{w}_{I_m^k,i+1} + \mathbf{w}_{T^k,i+1}\Big) + \mathbf{B}_0\mathbf{u}_{\tau,m,i}^k.
\end{aligned}$$

In the code-phase tracking the state vector contains the code-phase offset and its derivatives: $\Delta\tau_{m,i}^k,\ \Delta\dot{\tau}_{m,i}^k, \dots$. The offset is again the difference between the received signal and the locally generated copy (NCO-output). By using opposite signs for the ionospheric process-noise part in the carrier- and code-phase model, the loop accounts for the code-carrier-divergence.

The state-vectors of both, code- and carrier-phase, can now be stacked together. The outcomes of the discriminators are then related to the state as derived above and in the appendix. As a result the joint code and carrier tracking loop emerges.

OBSERVABILITY/CONTROLLABILITY

To successfully implement a controller for the plant describe in section 2, controllability and observability have to be fulfilled.

It can be shown that the observability matrix $\mathbf{Q}_o$ has rank $K\cdot M\cdot n$. Therefore observability after Kalman is fulfilled.

If n is larger than 2, the condition for controllability after Kalman can not be met. This can be seen from Equation 3, where matrix $\mathbf{B}_0$ shows empty rows. To solve this problem, either a higher order NCO could be used (not discussed here) or the higher order state-components are treated as a disturbance. In this case the disturbance is estimated by the observer and fed forward to the controller.

CONTROLLER DESIGN

Finally the feedback law of the controller takes the usual form of a linear controller:

$$\mathbf{u}_i = -\mathbf{K}\hat{\mathbf{x}}_i.$$

In contrast to a traditional PLL, both the phase and the frequency of the NCO could be steered, leading to more degrees of freedom in the choice of the controller. The poles of the controller can be selected directly by parametric state feedback design or by using results of optimal control, like described in [10], [12]. But with both design-approaches, the controller for every signal is only depending on the according state-components. Otherwise the control-system becomes unstable. Therefore, it can also be seen as a sort of decentralized control.

MULTICONSTELLATION TRACKING

Until now we have never made any assumption about the navigation system, except for the receiver's oscillator. Clearly this value has to be measured against a certain reference timescale. Assuming that the intersystem clock biases are many times more stable than the receiver's oscillator, the above model allows the joint tracking of satellites of multiple navigation systems. For example in the below described flight experiment, signals from GPS and GIOVE satellites are jointly tracked in one loop.

If the intersystem clock bias is not as stable as desired, it could optionally be included in the model in Equation 6. This would result in an additional remainder term, but no change in the state-vector.

3. RESULTS

This section shows performance results of the joint satellite tracking loop, based on a linearized baseband model (shown in Figure 1). We restrict ourselves to the case of carrier-phase tracking as it is usually more critical in a GNSS receiver than the code-phase tracking. Subsequently follows the evaluation of the joint code and carrier tracking algorithm for an airborne GNSS receiver.

PERFORMANCE COMPUTATIONS

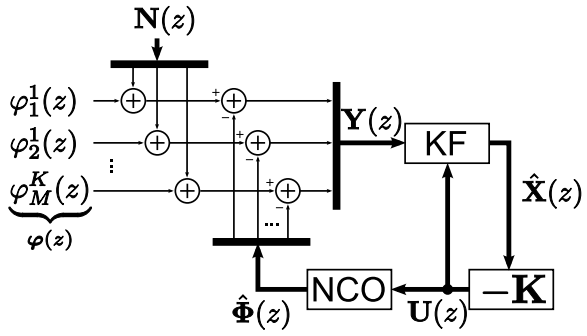

Fig. 1. Simplified baseband model of the joint satellite tracking loop (the bold lines represent vector quantities and the bars multi- and demultiplexing operations).

In [14] the transfer function between the input phase and measurement noise and the phase-error is derived. It consists of the transfer function of the NCO(s) ($\mathbf{H}_{\text{NCO}}(z)$) and that one of the estimator and controller ($\mathbf{H}_o(z)$):

$$\begin{aligned}\boldsymbol{\Delta}(z) &= \boldsymbol{\Delta}_{\varphi}(z) + \boldsymbol{\Delta}_n(z) \\ &= \underbrace{\left(\mathbf{I} + \mathbf{C}_p\mathbf{H}_{\text{NCO}}(z)\mathbf{H}_o(z)\right)^{-1}}_{\mathbf{H}_{\varphi}(z)}\boldsymbol{\varphi}(z) \\ &+ \underbrace{\mathbf{C}_p\mathbf{H}_{\text{NCO}}(z)\mathbf{H}_o(z)\left(\mathbf{I} + \mathbf{C}_p\mathbf{H}_{\text{NCO}}(z)\mathbf{H}_o(z)\right)^{-1}}_{\mathbf{H}_n(z)}\mathbf{N}(z),\end{aligned} \tag{9}$$

where $\boldsymbol{\Delta} = \boldsymbol{\varphi} - \hat{\boldsymbol{\varphi}}$ denotes the phase-error and $\mathbf{C}_p = \mathbf{I}_{K\cdot M} \otimes \mathbf{C}_2$ the measurement matrix for the whole state-vector.

Since the samples of the vector-valued noise process are white, the power spectral density of $\mathbf{N}(z)$ is a diagonal matrix, having in the diagonal the variances of the phase-discriminators:

$$S_{\mathbf{N}}(z) = \mathbb{E}\left\{\mathbf{n}_i\mathbf{n}_i^H\right\} = \tilde{\mathbf{R}},$$

where $(.)^H$ denotes the Hermitian transpose. We used a tilde for $\mathbf{R}$ here, to clarify the difference between the covariance matrix used in the loop evaluation here and the measurement covariance matrix used in the observer. Ideally they are the same. But especially in the low C/N_0-domain this must no longer be the case. Therefore the $\tilde{\mathbf{R}}$ represents the actual covariance of the samples.

Now the covariance of the noise-part of the carrier-error can be found by integrating its spectral density over one period:

$$\text{Cov}\left(\boldsymbol{\Delta}_n\right) = \frac{1}{2\pi}\int_{-\pi}^{\pi}\mathbf{H}_n\left(e^{j\Omega}\right)\tilde{\mathbf{R}}\mathbf{H}_n^H\left(e^{j\Omega}\right)d\Omega \tag{10}$$

In [15] it's shown that the standard deviation of the carrier-phase error – or also tracking jitter – marks a good measure for the mean time to cycle slipping in a PLL.

Meaning that the lower standard deviation the higher the robustness of the loop. Therefore the above value gives a good approximation of performance of the loop, especially in the higher C/N_0-domain, where the approximation of Equation 7 is valid.

Two analytical examples are presented here. In the first scenario, a static receiver is probed. The carrier-phase tracking performance of the joint tracking loop is compared to the individual Kalman filter tracking of all signals. The results are shown in Figure 2. Like mentioned

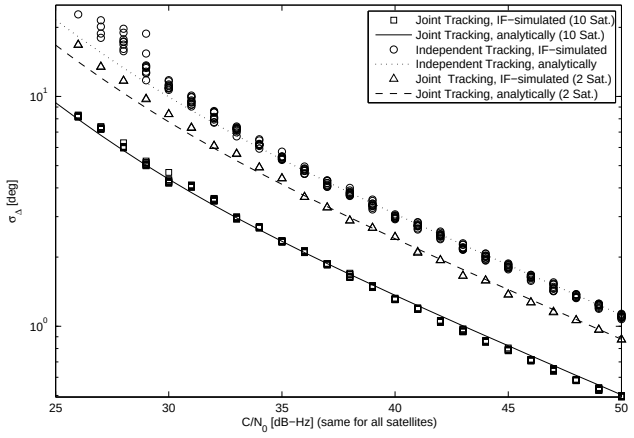

Fig. 2. Comparison of the performance of a multisatellite tracking loop (2 and 10 satellites) and traditional independent tracking loops.

above, the linearized baseband model is more precise in higher C/N_0-regions, where the additive noise assumption holds. To visualize the effect of this nonlinearity, the loops were also simulated in the intermediate-frequency (IF) domain. The carrier-to-noise density ratio drawn on the abscissa, in all cases stands for the strength of all signals.

The second scenario is a multifrequency Galileo receiver. Again the C/N_0 was used for all signals, i.e. all frequencies. It's performance evaluation is given in Figure 3.

The above two examples show the overall benefit of a joint satellite and/or joint frequency receiver. But usually not all satellites are affected by an attenuation concurrently (for example during ionospheric scintillation or – as later shown – aircraft maneuvers). Therefore the performance of a joint satellite tracking receiver is also evaluated for one failed satellite and 9 unaffected satellites. The analytic evaluation is conducted by using the formula in Equation 10 and displayed in Figure 3.

AIRCRAFT MEASUREMENTS

To test the joint code and carrier tracking algorithm, a test-flight with a Beechcraft King Air 350 airplane was conducted. The Antcom 42GO1116A2-XT-1 multifrequency

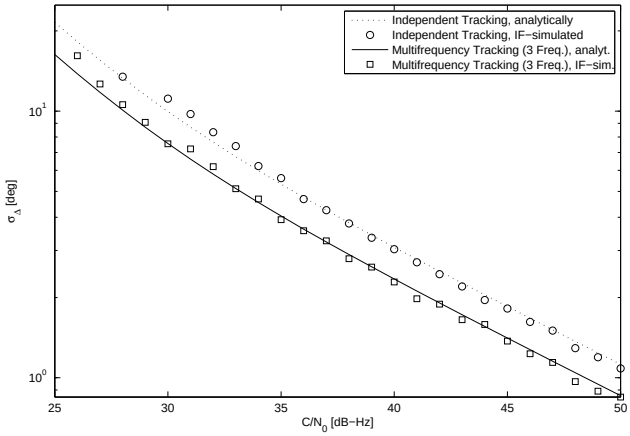

Fig. 3. Comparison of the performance of a multifrequency tracking loop (E1, E5a and E5b frequency) and traditional independent tracking loops.

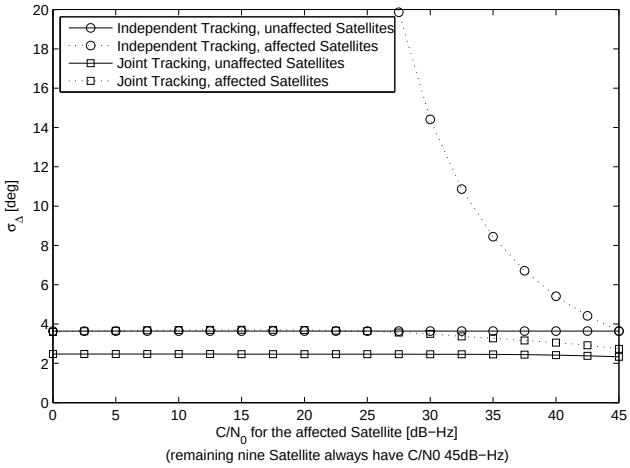

Fig. 4. Comparison of the carrier-phase tracking jitter for a scenario where one satetellite is strongly attenuated (abscissa). All other nine satellites remain unaffected at $45\,\mathrm{dB-Hz}$.

GNSS antenna was mounted on the roof, close to the cockpit (see Figure 5).

Fig. 5. Beechcraft King Air 350 airplane. The location of the antenna is shown by the arrow. The antenna follows the 743 ARINC configuration.

The first measurements were recorded during the enroute-flight between Braunschweig (Germany) and Innsbruck (Austria). The altitude of the aircraft was $28{,}000\,\mathrm{ft}$. Sig-

nals from 9 GPS satellites and the GIOVE-B satellite were received concurrently. To be able to compare the performance of the traditional and the joint-tracking loop in terms of robustness against individual signal outages, an artificial degradation of one satellite was implemented, see Fig. 6.

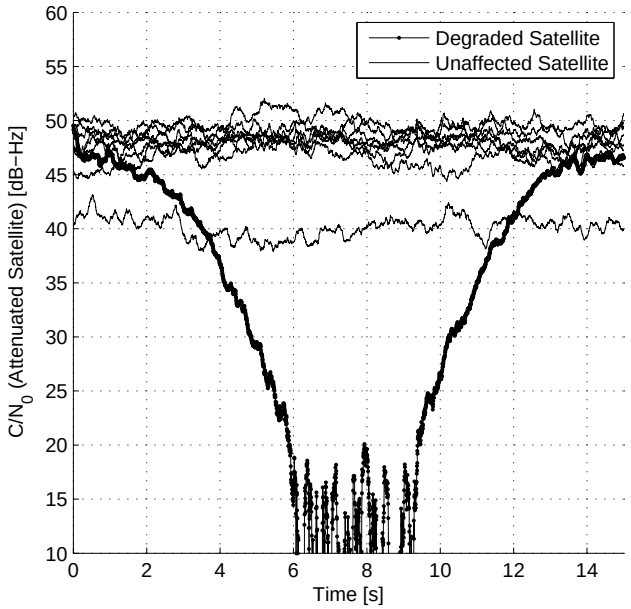

Fig. 6. C/N_0 for the artificially degraded and the unchanged satellites. Due to the increased variance in the low C/N_0-region, the estimated values between $6\,\mathrm{s}$ and $9\,\mathrm{s}$ are considered to be unreliable, but well below $15\,\mathrm{dB-Hz}$.

The comparison between an independent, traditional Kalman filter-based tracking scheme and the joint satellite tracking is given in Figure 7. In this case the reference was a carrier-phase estimate obtained by tracking the undegraded original data.

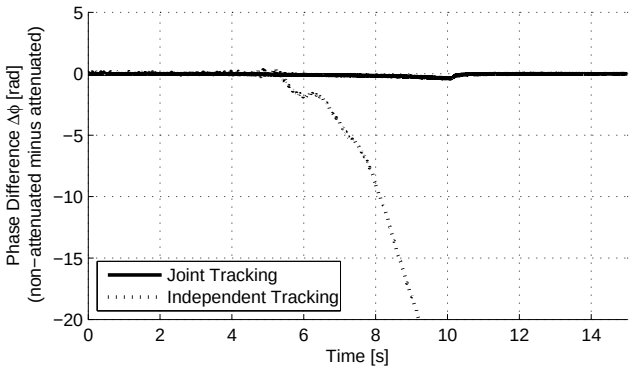

Fig. 7. Carrier-phase tracking error comparison of a traditional and joint satellite receiver with a strong attenuation of the considered satellite.

In addition to the enroute-flight a second measurement-run was recorded during a horizontal loop maneuver. To further exacerbate the conditions for the GNSS receiver, the maneuver was performed in the valley of the river Inn near Innsbruck (Austria), as can be seen from Figure 8. During this maneuver $11\,\mathrm{GPS}$ and the two GIOVE satellites were used in the receiver.

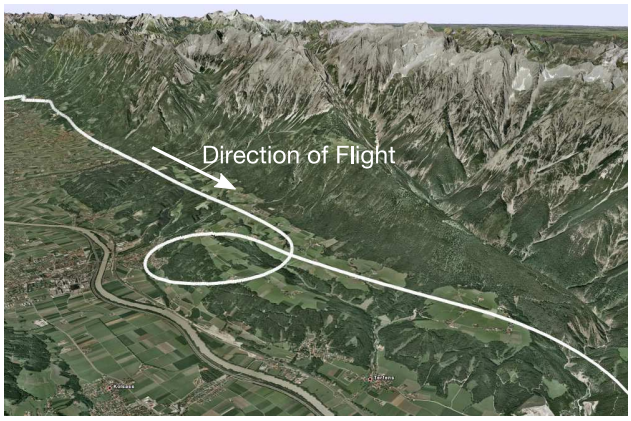

Fig. 8. Flight trajectory during the horizontal loop maneuver.

Clearly the geometry of the satellites changes during the maneuver due to their motion. But of course the impact is only very little at the receiver (less then one degree in the skyplot). On the other hand, due to the banking and turning of the aircraft, the geometry as actually seen by the antenna changes very rapidly. As an example, the skyplot corrected for the attitude of the receiver antenna is shown for the PRN 18 and GIOVE-A satellites (Fig. 9).

As can be seen, both of the considered satellites have a moderate initial elevation with respect to the antenna of $22\,^\circ$ and $36\,^\circ$ respectively. But during the maneuver the elevation drops down to negative values due to the attitude of the aircraft. The strong banking has two consequences. First, if the elevation falls below about $-5\,^\circ$ the wings of the airplane start to shadow the signal (depending on the azimuth-angle) and a strong attenuation of the signal results. Second, taking into account the hemispherical radiation pattern of the installed airborne antenna, signals of satellites having a negative elevation are attenuated.

How the attenuation, caused by the aircraft maneuvers, affects the tracking capabilities of an independent tracking receiver and a joint satellite tracking receiver, is shown in Figures 10 and 11. As a resource for the independent tracking receiver, a state-of-the-art commercial multifrequency, multiconstellation GNSS receiver was used. It was connected to the same antenna as the joint satellite tracking receiver, implemented in software for postprocessing.

Of course the curve of the aircraft results in line-of-sight accelerations and though in fast changing Doppler frequencies. This fact can be seen in Figures 10(c) and 11(c).

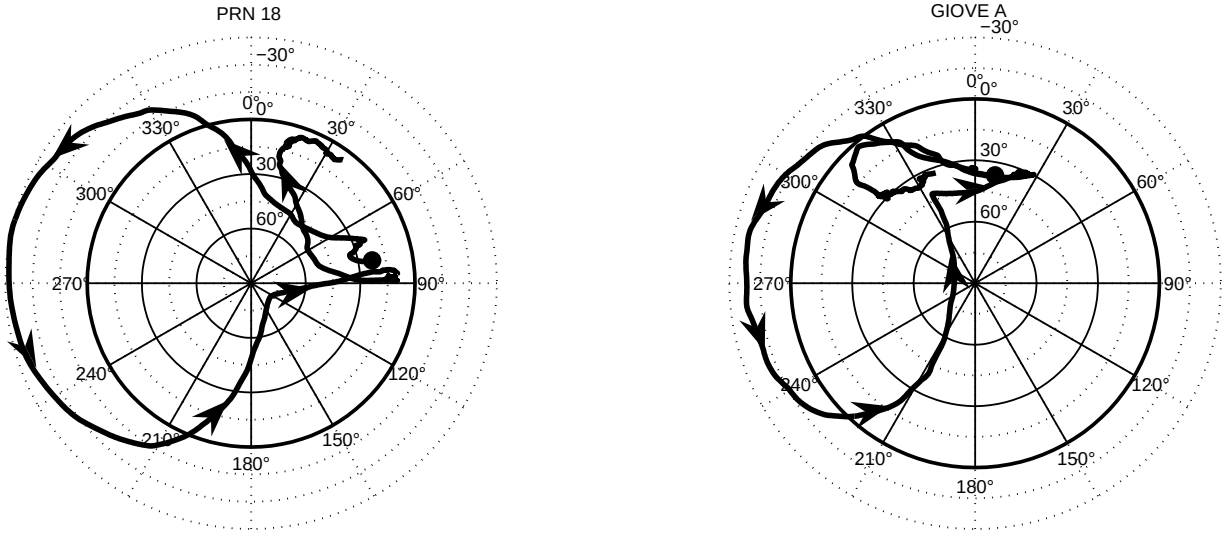

(a) GPS PRN 18 (b) GIOVE-A

Fig. 9. Skyplot corrected for the attitude of the antenna. The black dot marks the beginning of the maneuver and the arrows indicate the direction of the trajectory.

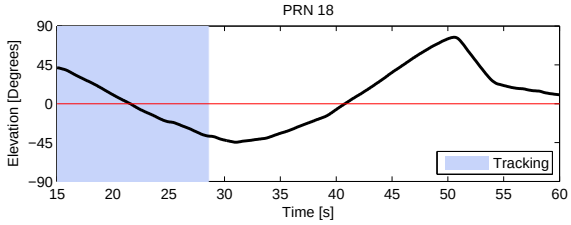

(a) Commercial receiver (independent tracking)

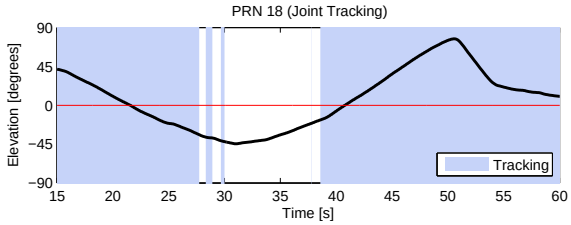

(b) Joint satellite tracking receiver

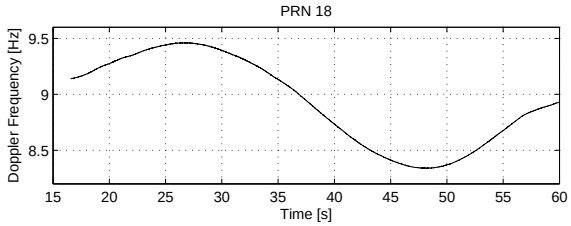

(c) Doppler frequency

Fig. 10. Elevation and lock versus time for satellite PRN 18. The shaded area represents the time of successful carrier tracking.

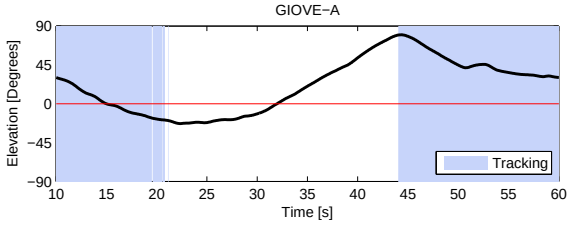

(a) Commercial receiver (independent tracking)

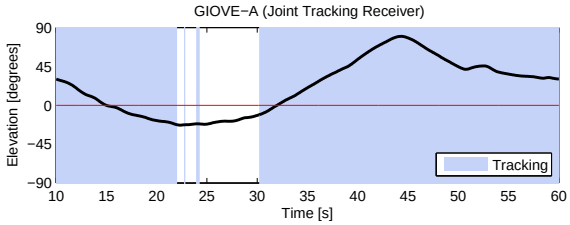

(b) Joint satellite tracking receiver

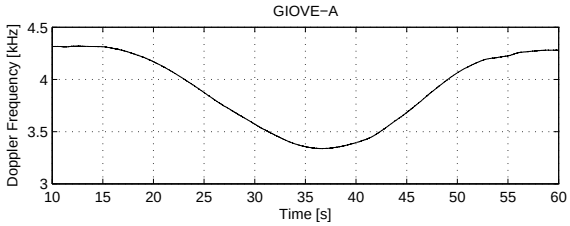

(c) Doppler frequency

Fig. 11. Elevation and lock versus time for satellite GIOVE-A. The shaded area represents the time of successful carrier tracking.

4. DISCUSSION

Three analytic evaluations have been presented in section 3. In Figures 2 and 3 the performance of a joint satellite and joint frequency tracking loop have been presented. They show the performances when all signals are affected the same way, i.e. all signals have the same carrier to noise density ratio. The third plot (Fig. 4) analyzes the situation where only one satellite is attenuated.

In the joint satellite case with 10 jointly tracked satellites, the gain compared to the independent tracking ranges from more than $8\,\mathrm{dB-Hz}$ at high C/N_0 to about $5\,\mathrm{dB-Hz}$ for weaker signals. If only two satellites are tracked jointly, the gain can be found to be approximately $3\,\mathrm{dB-Hz}$. Summarizing the joint satellite case, we can find that the upper limit of the achievable gain is given by the formula $G_{K\text{ sat.}} \leq 10\log_{10}(K)$, where K denotes the number of satellites tracked jointly.

The analysis of the joint frequency tracking case shows a somewhat similar result. The biggest gain is achieved for low noise, in the case of the three Galileo frequencies (E1, E5a, E5b) about $4\,\mathrm{dB-Hz}$. The gain is a bit less for weaker signals ($\approx 3\,\mathrm{dB-Hz}$). So again an upper bound can be found to read $G_{M\text{ freq.}} \leq 10\log_{10}(M)$, where M denotes the number of frequencies tracked jointly.

In the three figures discussed above, the intermediate-frequency analysis shows a little deviation from the analytic expression, when signals have a low C/N_0. The reason is basically the nonlinearity of the discriminator whose impact is increased with higher noise. But altogether both IF-simulations and analytic evaluations show the same behavior and trends. They allow us to define a general upper limit for the performance gain of a joint tracking loop over a traditional independent tracking loop:

$$G_{K\text{ sat.},\ M\text{ freq.}} \leq 10 \cdot \log_{10}\left(K \cdot M\right).$$

The maybe more common situation where only one (or at most few) satellites suffer from strong attenuation or masking was shown in Figure 4. We know from several publications the shape of the phase jitter curve plotted against the carrier to noise density ratio. Therefore we're not surprised to see this shape again, when looking at the curve for the affected satellite in the independent tracking case. In the joint satellite case the carrier-phase jitter of the attenuated satellite is slowly increased if its C/N_0 decreases. But it always stays well below the usually considered tracking-threshold of $15\,^\circ$. On the other hand, clearly the performance of the unaffected satellites must be lower if one satellite has a very weak signal. But due to the low weighting of the according satellite, the performance penalty is negligible, as also indicated in the plot.

The three discussed figures show the great potential of the joint satellite and frequency tracking algorithm. In both situations, if only a few satellites are masked or attenuated as well if the signals from all satellites in view are weak, the joint tracking receiver improves the performance of the GNSS receiver. The first case is especially helpful in the case of scintillation or banking in an aircraft, the second case for example in indoor environments.

To test the found results, the flight-measurements were shown in the second part of section 3. The enroute example, where one satellite was artificially attenuated, represents the situation discussed above. Taking Figure 4 into account, a joint tracking receiver should be able to continuously track the carrier-phase also of the masked satellite. Figure 7 shows that this is indeed the case. This means that a joint satellite tracking receiver can cope with signal-outages of a few seconds without leading to a loss-of-lock or even cycle slip, also with real measurement data.

The horizontal loop maneuver represents a more difficult case since more than one satellite fails concurrently. As can be seen, the commercial receiver needs some few seconds to recover the signals of the lost satellites in the case of GIOVE-A. Looking at the PRN 18 satellite, the receiver completely fails to re-acquire the signal during more than a minute. One of the reasons for this behavior can be seen from the Doppler plots. During the outage (or very low satellite elevation, as seen by the antenna) the Doppler frequency substantially changes. Starting afterwards with the phase tracking loop again won't work as on one side the signal has left the pull-in region of the PLL. And on the other side the code was lost and therefore the DLL cannot be just restarted again. Therefore the traditional receiver needs a complete re-acquisition which takes some time. In contrast to the commercial receiver, the joint satellite tracking receiver can recover the signal as soon as its C/N_0 exceeds a certain threshold. Actually the signal is continuously tracked, therefore the shaded area, representing the time of tracking, is found by considering the phase lock indicator.

5. CONCLUSION

The joint satellite code and carrier tracking loop shows to greatly improve the performance of a GNSS receiver in terms of tracking jitter and availability of satellites. Whenever few satellites are lost due to masking, ionospheric effects or the like, the joint satellite tracking receiver avoids the re-acquisition and recovers the signal as soon it becomes available again, as shown in this paper by using an airborne GNSS receiver. Furthermore it was indicated that even cycle slips could be avoided. Therefore the joint tracking loop enhances the robustness of a GNSS receiver.

6. ACKNOWLEDGMENTS

The authors would like to thank the German Federal Ministry of Economic Affairs and Technology (BMWi) and the German Aerospace Center (DLR) for a financial grant (FKZ: 50NA0911).

* REFERENCES

[1] E. D. Kaplan and C. J. Hegarty, Eds., *Understanding GPS – Principles and Applications*, 2nd ed. Artech House, 2006.

[2] J. Seo, T. Walter, T.-Y. Chiou, and P. Enge, "Characteristics of deep GPS signal fading due to ionospheric scintillation for aviation receiver design," *Radio Science*, vol. 44, 2009.

[3] P. Henkel, V. Gomez, and C. Günther, "Modified LAMBDA for absolute carrier phase positioning in the presence of biases," in *Proceedings of the Internationl Technical Meeting (ITM)*. Anaheim: Institute of Navigation (ION), Jan 2009, pp. 642–651.

[4] J. W. Sennott and D. Senffner, "The use of satellite constellation geometry and a priori motion constraints for prevention of cycle slips in a GPS signal processor," *NAVIGATION, Journal of the Institute of Navigation*, vol. 39, no. 2, pp. 217 – 236, 1992.

[5] B. W. Parkinson and J. J. S. Jr., *Global Positioning System: Theory and Applications*. Progress in Astronautics and Aeronautics, 1996, vol. Volume I.

[6] T. Pany, R. Kaniuth, and B. Eissfeller, "Deep integration of navigation solution and signal processing," in *Proceedings of the ION GNSS 18th International Technical Meeting of the Satellite Division*, Long Beach, CA, September 2005.

[7] P. Henkel, K. Giger, and C. Gunther, "Multifrequency, multisatellite vector phase-locked loop for robust carrier tracking," *Selected Topics in Signal Processing, IEEE Journal of*, vol. 3, no. 4, pp. 674–681, Aug. 2009.

[8] M. L. Psiaki and H. Jung, "Extended Kalman filter methods for tracking weak GPS signals," in *Proceedings of the 15th International Technical Meeting of the Satellite Division of the Institute of Navigation ION GPS 2002*, Oregon, September 2002, pp. 2539–2553.

[9] A. Patapoutian, "On phase-locked loops and Kalman filters," *IEEE Transactions on Communications*, vol. Volume 47, no. 5, pp. 670–672, May 1999.

[10] G.-I. Jee, "GNSS receiver tracking loop optimization for combined phase, frequency and delay locked loops," in *Proceedings of the European Navigation Conference ENC – GNSS 2005*, Munich, July 2005.

[11] R. G. Brown and P. Y. C. Hwang, *Introduction to Random Signals and Applied Kalman Filtering*. John Wiley & Sons, Inc., 1992.

[12] C. O'Driscoll and G. Lachapelle, "Comparison of traditional and Kalman filter based tracking architectures," in *Proceedings of the European Navigation Conference ENC – GNSS 2009*, Naples, May 2009.

[13] V. A. Vilnrotter, S. Hinedi, and R. Kumar, "Frequency estimation techniques for high dynamic trajectories," *IEEE Transactions on Aerospace and Electronic Systems*, vol. Volume 25, no. 4, July 1989.

[14] K. Giger, P. Henkel, and C. Günther, "Multifrequency multisatellite carrier tracking," in *Proceedings of the Fourth European Workshop on GNSS Signals and Signal Processing*, Dec 2009.

[15] W. C. Lindsey, *Synchronization Systems in Communication and Control*. Englewood Cliffs, NJ: Prentice-Hall, Inc., 1972.

[16] S. J. Julier and J. K. Uhlmann, "A new extension of the Kalman filter to nonlinear systems," in *Society of Photo-Optical Instrumentation Engineers (SPIE) Conference Series*, 1997, pp. 182–193.

APPENDIX

The Inphase- and Quadrature-components at the output of the correlators can be approximated as in [5]:

$$I_i \approx D_i R(\Delta\tau_i) \cdot \operatorname{sinc}\left(\frac{T}{2} \cdot \overline{\Delta\omega_i}\right) \cdot \cos\left(\overline{\Delta\varphi_i}\right) + n_{I,i},$$

$$Q_i \approx D_i R(\Delta\tau_i) \cdot \operatorname{sinc}\left(\frac{T}{2} \cdot \overline{\Delta\omega_i}\right) \cdot \sin\left(\overline{\Delta\varphi_i}\right) + n_{Q,i},$$

where $\overline{\Delta\omega_i}, \overline{\Delta\varphi_i}$ are the average frequency and phase offsets respectively, during the interval $[t_{i-1}, t_i]$, and $n_{I,i}, n_{Q,i}$ are zero-mean, uncorrelated Gaussian noise samples of variance $1/(2C/N_0T)$.

Using the arctangent-discriminator $D_i = \operatorname{atan}(Q_i/I_i)$, the noise is no more additive, especially in the low C/N_0 region. Due to this violation of the assumptions of the Kalman filter, the measurement noise can also be treated nonlinearly by augmenting the state-vector with the measurement noise samples and by employing and Extended Kalman filter [16]:

$$\tilde{\mathbf{x}}_{i+1} = \begin{bmatrix} \mathbf{x}_{i+1} \\ n_{I,i+1} \\ n_{Q,i+1} \end{bmatrix} = \underbrace{\begin{bmatrix} \mathbf{A} & \mathbf{0} \\ \mathbf{0} & \mathbf{0} \end{bmatrix}}_{\tilde{\mathbf{A}}} \tilde{\mathbf{x}}_i + \underbrace{\begin{bmatrix} \mathbf{w}_{i+1} \\ n_{I,i+1} \\ n_{Q,i+1} \end{bmatrix}}_{\tilde{\mathbf{w}}_{i+1}}.$$

The measurements, i.e. discriminator outputs, are related to the states by the nonlinear function

$$D_i = \tilde{c}\left(\tilde{\mathbf{x}}_i, v_i\right) = \operatorname{atan}\left(Q_i/I_i\right) + v_i.$$

In the present case the measurement noise is already contained in I_i, Q_i and therefore $\mathbb{E}\{v_i v_j\} = R_v = 0$. On the other hand the process-noise covariance matrix is now consisting also of the $n_{I,i}$ and $n_{Q,i}$:

$$\mathbb{E}\left\{\tilde{\mathbf{w}}_i \tilde{\mathbf{w}}_j^T\right\} = \delta(i-j) \cdot \underbrace{\begin{bmatrix} \mathbf{Q} & \mathbf{0} \\ \mathbf{0} & \mathbf{Q}_n \end{bmatrix}}_{\tilde{\mathbf{Q}}}$$

$$\text{and } \mathbf{Q}_n = \frac{1}{2C/N_0T} \cdot \mathbf{I}_2$$

In the iteration-equations of the EKF, the update for the Kalman gain is instead of $\hat{\mathbf{P}}_i^- \mathbf{C}\left(\mathbf{C}\hat{\mathbf{P}}_i^- \mathbf{C}^T + R_i\right)^{-1}$ now:

$$\tilde{\mathbf{K}}_i = \hat{\tilde{\mathbf{P}}}_i^- \mathbf{J}_{\tilde{c}}\left(\hat{\tilde{\mathbf{x}}}_i^-\right) \cdot \left[\mathbf{J}_{\tilde{c}}\left(\hat{\tilde{\mathbf{x}}}_i^-\right) \hat{\tilde{\mathbf{P}}}_i^- \mathbf{J}_{\tilde{c}}^T\left(\hat{\tilde{\mathbf{x}}}_i^-\right) + 0\right]^{-1},$$

where the Jacobian of $\tilde{c}(\mathbf{x})$ is defined as $\partial\tilde{c}(\mathbf{x})/\partial\mathbf{x}$. Because of the shape of the state-transition matrix $\tilde{\mathbf{A}}$, the a priori estimated state vector will always be $\hat{\tilde{\mathbf{x}}}_i^- = \left[\left(\hat{\mathbf{x}}_i^-\right)^T,\ 0,\ 0\right]^T$. Plugging in the a priori estimate, the Jacobian reads

$$\mathbf{J}_{\tilde{c}}\left(\hat{\tilde{\mathbf{x}}}_i^-\right) = \left[\ \mathbf{C},\quad -\frac{\sin\left(\overline{\Delta\varphi_i}\right)}{\operatorname{sinc}^2\left(\overline{\Delta\omega_i}\frac{T}{2}\right)},\quad \frac{\cos\left(\overline{\Delta\varphi_i}\right)}{\operatorname{sinc}^2\left(\overline{\Delta\omega_i}\frac{T}{2}\right)}\ \right].$$

Using the above result and the shape of the $\tilde{\mathbf{A}}$-matrix, the matrix to be inverted for the Kalman gain can be evaluated:

$$\mathbf{J}_{\tilde{c}} \hat{\tilde{\mathbf{P}}}_i \mathbf{J}_{\tilde{c}}^T = \mathbf{C}\hat{\mathbf{P}}_i^- \mathbf{C}^T + \underbrace{\frac{1}{\operatorname{sinc}^2\left(\overline{\Delta\omega_i}\frac{T}{2}\right)} \cdot \frac{1}{2C/N_0T}}_{R_\varphi}. \quad (11)$$

The result in Equation 11 encourages us to use $1/(2C/N_0T)$ for the measurement covariance matrix, since in the lock case the term $1/\operatorname{sinc}^2(\overline{\Delta\omega} \cdot T/2)$ is close to 1. In a similar way the measurement covariance matrix for the code discriminator can be found.